14th International Conference on Structural Safety and Reliability - ICOSSAR'25
1-6 June, 2025 - Los Angeles California, USA
R. Ghanem, E. Johnson, S. Masri and A. Olivier (Eds)

SIMULATION METHOD FOR THE SPATIAL DISTRIBUTION OF SEISMIC INTENSITY ON ENGINEERING BEDROCK FOR REAL-TIME EARTHQUAKE DISASTER RISK ESTIMATION

YUNA TANAKA[1], AKIRA AKAMATSU[2], MICHIYO SUGAI[3] AND YASUHIRO MORI[4]

[1]Graduate School of Environmental Studies, Nagoya University
Furo-cho, Chikusa-ku, Nagoya, Japan, 464-8603
bj.51m.3368@s.thers.ac.jp

[2] Graduate School of Environmental Management, Nagoya Sangyo University
Yamanota-3255-5, Arai-cho, Owariasahi, Aichi, Japan, 488-8711
a-akamatsu@nagoya-su.ac.jp

[3]Graduate School of Environmental Management, Nagoya Sangyo University
Yamanota-3255-5, Arai-cho, Owariasahi, Aichi, Japan, 488-8711
sugai@nagoya-su.ac.jp

[4]Nagoya University
Furo-cho, Chikusa-ku, Nagoya, Japan, 464-8603
yasu@nuac.nagoya-u.ac.jp

Key words: seismic intensity, spatial distribution, engineering bedrock, Kriging analysis.

1 INTRODUCTION

This study proposes a method for accurately estimating the spatial distribution of seismic intensity on engineering bedrock in real-time. Developing a system that can assess seismic damage risk for individual buildings is imperative for mitigating earthquake-related damage. By incorporating this system into a simulator and considering various hypothetical epicenters and conditions, it can be utilized for both evacuation drills and earthquake preparedness. Seismic risks—such as the risk of total building collapse—can be estimated based on the seismic intensity at the ground surface and the seismic performance level of the building[1]. However, the seismic intensity at the ground surface varies significantly depending on the condition of the surface layer beneath each building; hence, a substantial number of seismometers would be required to estimate intensity at every building site through spatial interpolation. For most municipal governments, the cost of installing and maintaining such a dense network of seismometers is prohibitive[2]. Conversely, the spatial distribution of seismic intensity on engineering bedrock can be estimated using a relatively small number of seismometers because spatial variation is much smaller than that observed at the ground surface[3].

Increasing amounts of seismic intensity data on engineering bedrock are available through seismometers installed by institutions such as the National Research Institute for Earth Science and Disaster Resilience. Another study is underway to develop a method for estimating ground-surface seismic intensity from that on engineering bedrock, using site-specific amplification factors. These amplification factors can be estimated via spatial interpolation, based on borehole data from a sufficiently large number of locations[4–7]. By applying this method, once the seismic intensity at a point on engineering bedrock is known, the corresponding ground surface intensity can also be estimated. However, the spatial distributions of seismic intensity on engineering bedrock have not yet been examined from a statistical perspective. The author propose a method for estimating the spatial distribution of seismic intensity on engineering bedrock after an earthquake, using seismic records from a limited number of seismometers installed on the bedrock surface.

2 METHOD FOR EVALUATING SEISMIC INTENSITY AT ARBITRARY POINTS ON ENGINEERING BEDROCK

In this study, the Universal Kriging method was employed to estimate the spatial distribution of seismic intensity on the engineering bedrock surface[8,9]. The trend function in the Universal Kriging analysis was defined as

$$\mu(u) = b_0 + b_1 x + b_2 y + b_3 x^2 + b_4 xy + b_5 y^2 + \cdots + b_{m_b} y^n \tag{1}$$

where x and y represent the coordinates of the location u, n is the degree of the polynomial, and b_i denote the coefficients that define the trend function. The total number of elements in the coefficient vector $\boldsymbol{b}$, denoted as m_b, is given by $m_b = \frac{(n+1)\cdot(n+2)}{2}$.

Additionally, the elements σ_{ij}^2 of the variogram function θ, representing the covariance matrix in the Kriging analysis, were modeled using the following general exponential function:

$$\sigma^2{}_{ij} = \sigma^2 \exp\left(-\frac{h_{ij}}{\ell}\right) \tag{2}$$

where σ^2 represents sill, h_{ij} denotes the distance between point i and j, and ℓ is range.

The optimal polynomial degree, coefficient vector, and variogram parameters were determined by minimizing the Akaike Information Criterion (AIC)[10]:

$$\min_{\mu,\theta,m} AIC = -2 \times Max\{\ln p(z\,|\mu,\theta)\} + 2 \times (m) \tag{3}$$

where $\boldsymbol{z}$ is the vector of parameters to estimate the spatial distribution, $\mathrm{Max}\{\ln p(\boldsymbol{z}|\mu,\theta)\}$ represents the maximum log-likelihood, and m denotes the total number of explanatory variables in the variogram function and the trend function. The variogram function has two explanatory variables—sill and range—and the trend function has $m_b = \frac{(n+1)\cdot(n+2)}{2}$ explanatory variables. Thus, m =2+$\frac{(n+1)\cdot(n+2)}{2}$.

In a Universal Kriging analysis, the target area is modeled as a random field, where the values of the parameters at both sample points and interpolation points comprise two components: a trend component, which describes the approximate spatial distribution of the parameters, and a random component, which accounts for the location-dependent random variation in the parameters [11]. When a random field follows a log-normal distribution, the parameter is expressed as the product of the trend and random components.

In this study, the time-dependent Fourier spectral intensity (FSI), defined by Eq. (4), was employed as seismic intensity and considered a target parameter of the estimation[12].

$$FSI = \int_{T_1}^{3.5T_1} FS(T)dT \tag{4}$$

where $FS(T)$ is Fourier amplitude spectrum of a ground motion, and T_1 is the natural period of a wooden house, which can be estimated by

$$T_1 = 0.31 \times I_g^{-0.687} \tag{5}$$

where I_g is an index representing the seismic performance of a house, obtained through I_g in seismic diagnosis. Assuming that FSI follows a log-normal random field, z in Eq. (3) is replaced by FSI. The trend component is assumed to vary with earthquake source characteristics, while the random component—the compensation ratio—is assumed to be site-specific and independent of the source. Under this assumption, the trend value at each seismic observation point can be estimated by dividing the observed FSI by the compensation ratio. The trend distribution across the entire area is then estimated using the least squares method. Finally, the FSI at any arbitrary point on the engineering bedrock can be obtained by multiplying the trend value by the corresponding compensation ratio.

3 SPATIAL DISTRIBUTIONS OF SEISMIC INTENSITY IN AICHI PREFECTURE

3.1 Seismic intensity for each 250-m mesh

The natural period T_1 typically ranges from 0.2 to 1.0 s for most conventional wooden houses. In this study, owing to space limitations, FSI of T_1 = 0.2 s is used as a representative example.

Following the 2011 Great East Japan Earthquake, Japanese government research committees simulated six types of seismic waves on engineering bedrock across Japan, based on three Nankai Trough earthquake scenarios: the Last-ever, East-side, and Land-side epicenter models[13]. These simulations provided 50-Hz digital seismic-wave data for each of the 80,396, 250 m × 250 m, mesh cells in Aichi Prefecture (total area: 5,172.92 km²); however, 1,263 data points were missing for the East-side model. The FSI values calculated from these seismic waves using Eq. (4) are referred to as FSI_o.

Figure 1 (a)–(c) illustrate the spatial distribution of FSI_o across Aichi Prefecture. The left-hand figures show the North–South components of ground motion, while the right-hand figures show the East–West components. These distributions vary depending on the epicenter model and the direction of ground motion.

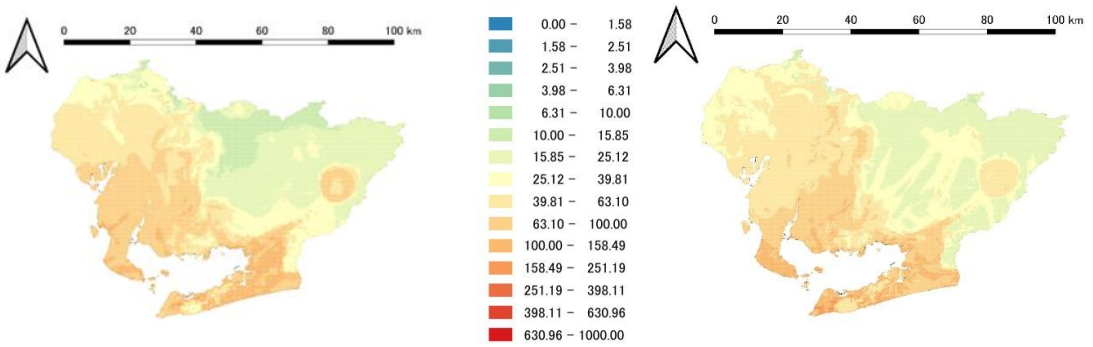

(i) (North–South direction) (ii) (East–West direction)

(a)

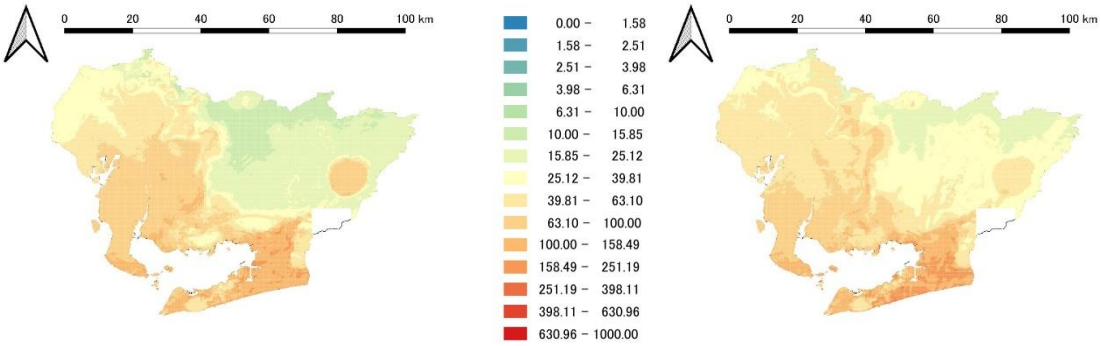

(i) (North–South direction) (ii) (East–West direction)

(b)

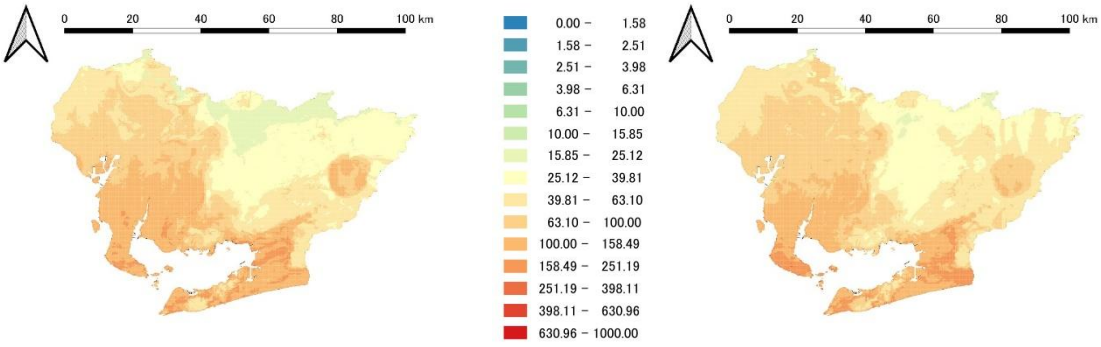

(i) (North–South direction) (ii) (East–West direction)

(c)

Figure 1: Special distribution of FSI_o of (a) Last-ever epicenter model, (b) East-side epicenter model, and (c) Land-side epicenter model of Nankai Trough massive earthquakes

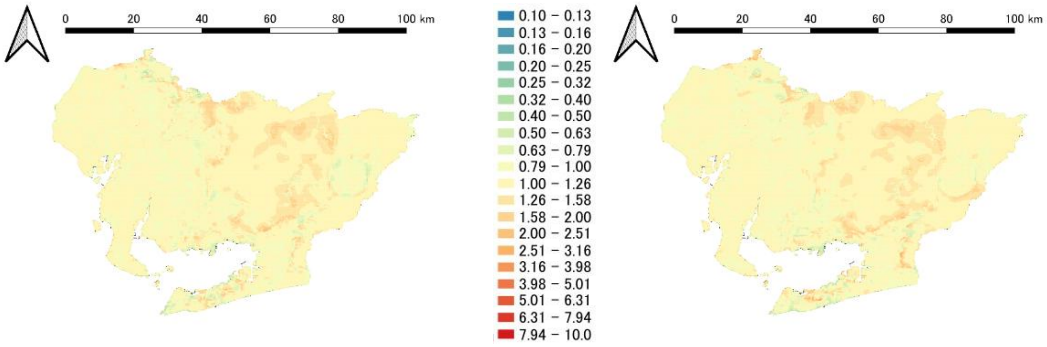

(i) (North–South direction) (ii) (East–West direction)

(a)

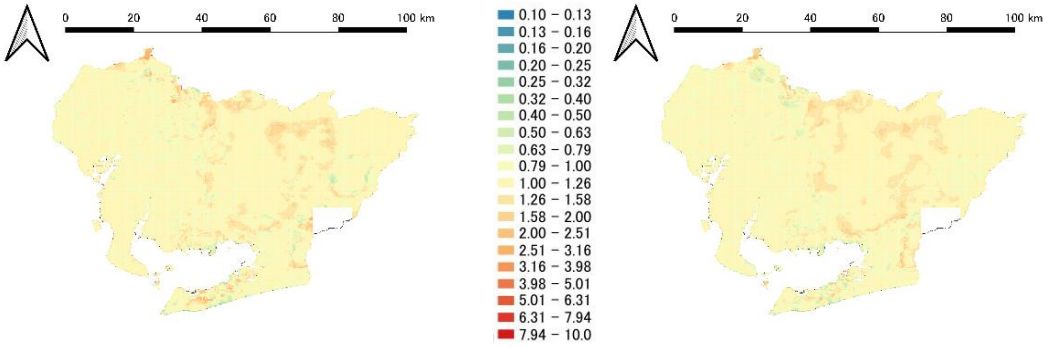

(i) (North–South direction) (ii) (East–West direction)

(b)

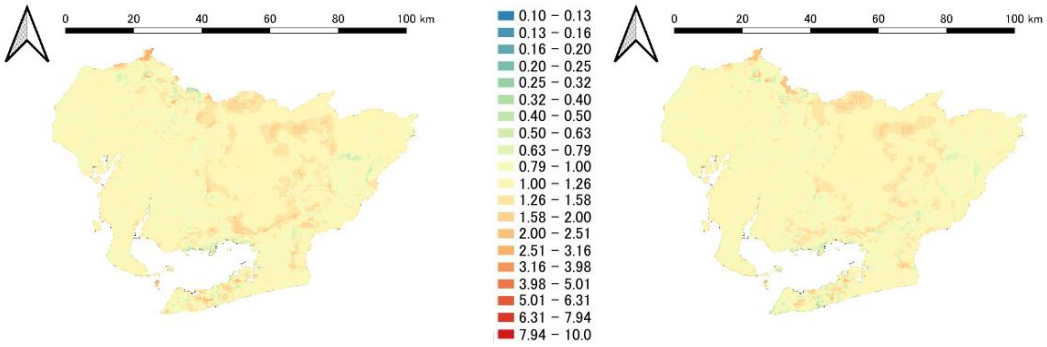

(i) (North–South direction) (ii) (East–West direction)

(c)

Figure 2: Special distribution of the ratio of FSI_e to FSI_o of (a) Last-ever epicenter model, (b) East-side epicenter model, and (c) Land-side epicenter model of Nankai Trough massive earthquakes

3.2 Spatial distribution by Kriging analysis using the values at sample points

In this study, Kriging analysis was used to simulate the spatial distribution of FSI, and both trend and random components (referred to as compensation ratios) were estimated.

Ideally, all FSI values at approximately 80,000 mesh points in Aichi Prefecture should be used for accurate Kriging analysis. However, owing to computational constraints, this was not feasible. Therefore, a subset of approximately 2,500 mesh points was selected for the analysis.

To reduce the dataset from over 80,000 to approximately 2,500 points, mesh cells exhibiting local maxima or minima within a 5×5 mesh neighborhood were chosen as sample points. In conventional Kriging, the values at sample points are exactly reproduced, while interpolated values fall between those of nearby samples. By selecting local extrema as sample points, the interpolated values were more likely to lie between true peaks and troughs, thereby reducing estimation errors at unsampled locations.

3.3 Results of Kriging analysis and their validity

AICs were calculated for six seismic waves using polynomial trend functions of degrees 0 to 7 to determine the optimal degree based on Eq. (3). The analysis revealed that the optimal degree of the trend function that minimizes the AIC is either five or six, regardless of the source and direction. From the perspective of information criterion statistics, performing interpolation using the trend function with this optimal degree is desirable. However, as given in Eq. (1), at least 21 observation points with seismometers are required to estimate a fifth- or sixth-degree trend function using the least squares method. Currently, however, there are only approximately 20 seismometers installed on the engineering bedrock surface within Aichi Prefecture. Therefore, spatial distributions of FSI_o were simulated using a fourth-degree trend function.

Notably, the estimated range values ℓ typically fall between 1,500 m and 2,000 m when a fourth-degree trend function is utilized. These values are significantly larger than the 250-m mesh spacing between sample points, which indicates that the interpolation is not adversely affected by spatial resolution limitations. The accuracy of reproducing the spatial distribution of FSI across the entire area of Aichi Prefecture was verified using a limited number of sample points (2500).

The FSI estimated by Kriging interpolation with the 2500 sample points is referred as FSI_e and is compared with the FSI_o of the six spatial distributions shown in Figure 1.

Table 1: Summary of Statistics of FSI_e and FSI_o in Figure 5

Epicenter Model and Direction Statistics	Last-ever		East-side		Land-side	
	North–South	East–West	North–South	East–West	North–South	East–West
Average of ratio of FSI_e to FSI_o	1.071	1.076	1.063	1.057	1.078	1.060
Coefficient of variation of ratio of FSI_e to FSI_o	0.166	0.167	0.168	0.151	0.171	0.156
Correlation coefficient of FSI_e and FSI_o	0.962	0.941	0.963	0.954	0.957	0.955

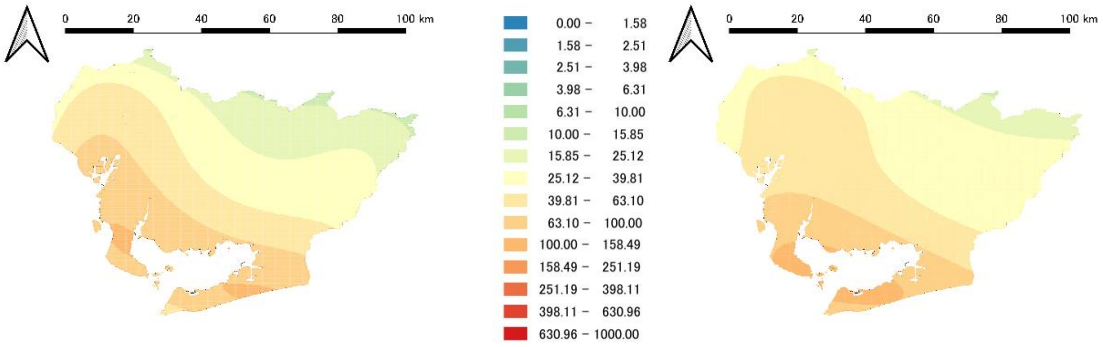

(i) (North–South direction) (ii) (East–West direction)

(a)

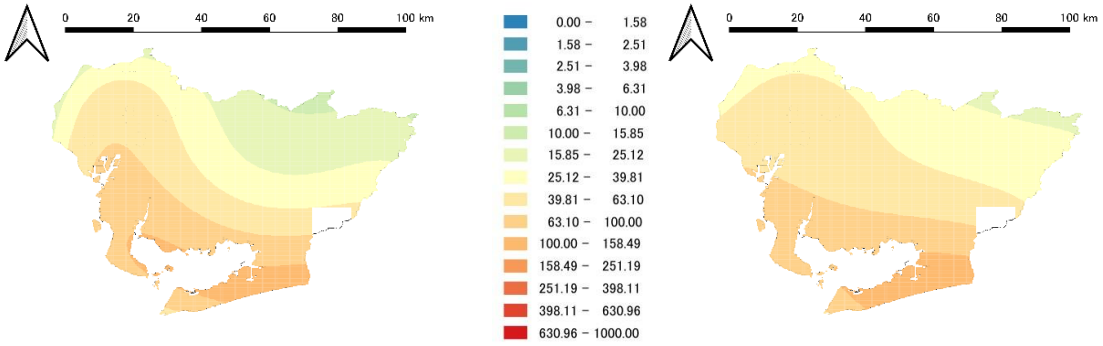

(i) (North–South direction) (ii) (East–West direction)

(b)

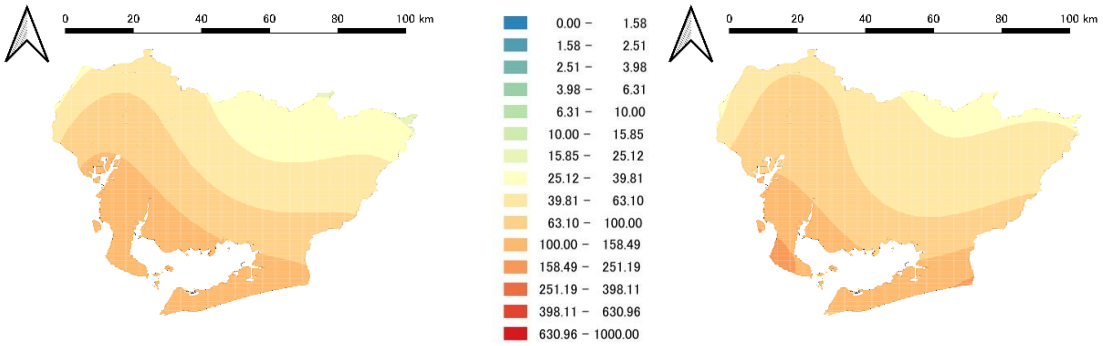

(i) (North–South direction) (ii) (East–West direction)

(c)

Figure 3: Special distribution of trend function of FSI_o of (a) Last-ever epicenter model, (b) East-side epicenter model, and (c) Land-side epicenter model of Nankai Trough massive earthquakes (degree of the polynomial = 4)

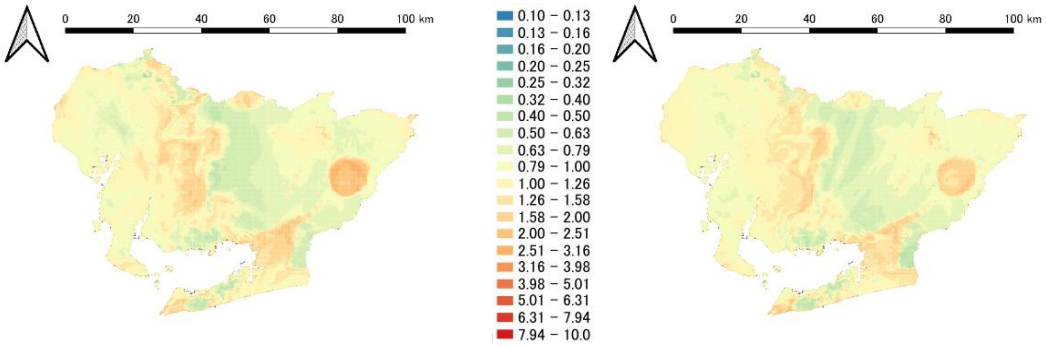

(i) (North–South direction) (ii) (East–West direction)

(a)

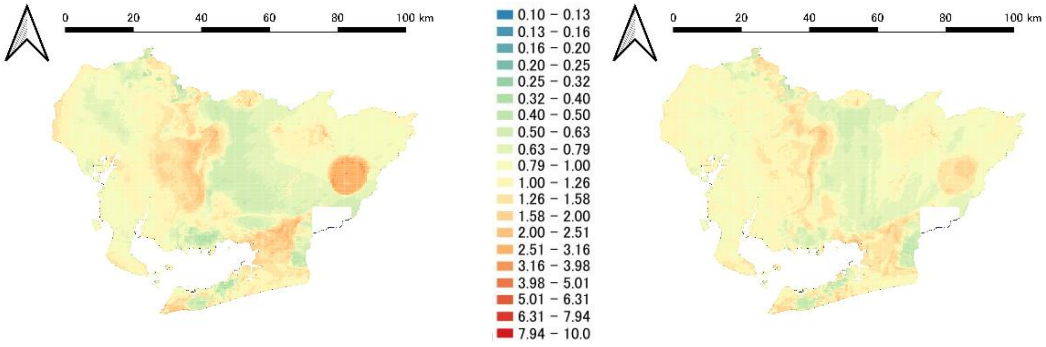

(i) (North–South direction) (ii) (East–West direction)

(b)

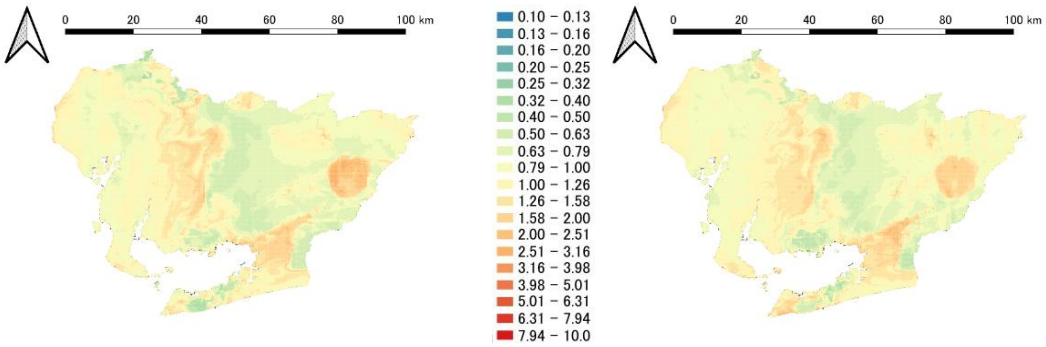

(i) (North–South direction) (ii) (East–West direction)

(c)

Figure 4: Special distribution of compensation ratio of (a) Last-ever epicenter model, (b) East-side epicenter model, and (c) Land-side epicenter model of Nankai Trough massive earthquakes

Figure 2 (a)–(c) illustrate the spatial distribution of the ratio FSI_e, / FSI_o. As demonstrated, these ratios are close to 1.0 across nearly all locations, regardless of the epicenter model or direction of seismic waves.

Table 1 summarizes the statistics of the ratio of FSI_e to FSI_o illustrated in Figure 1 along with the coefficient of variation between FSI_e and FSI_o. The averages of the ratio are almost 1.0, the coefficients of variation of the ratio are distributed from 0.151 to 0.171, and the correlation coefficient between FSI_e and FSI_o is almost 1.0. These statistical values were calculated without the data from the 2500 sample points.

Figure 2 and Table 1 show that FSI_o is well represented in all areas of Aichi prefecture by the FSI_e, which is estimated using the 2500 sample data points. Thus, both the trend and random components (compensation ratio) can be considered to be accurately estimated at all meshes in Aichi prefecture using only the 2500 sample data points.

4 TRENDS AND COMPENSATION RATIOS

4.1 Distributions of trends and compensation ratios

Figure 3 (a)–(c) illustrates the trend distributions modeled using fourth-degree polynomial functions. As demonstrated, these distributions vary depending on the epicenter model and the direction of seismic waves.

Figure 4 (a)–(c) presents the distributions of the compensation ratios, which were obtained by dividing FSI_o by the corresponding trend distributions illustrated in Figure 3 (a)–(c). While the trend distributions differ significantly across the six cases, the compensation ratio distributions appear nearly identical, regardless of the epicenter model or wave direction.

4.2 Averages and variations of the compensation ratios in their spatial distributions

Figure 5 shows the spatial distribution of the mean values of the six compensation ratios presented in Figure 4. This distribution closely resembles those shown in Figure 4. Notably, the average compensation ratios range widely from approximately 0.35 to 2.42; this indicates that seismic intensity cannot be accurately estimated using trend distributions alone; compensation ratios at each location are essential.

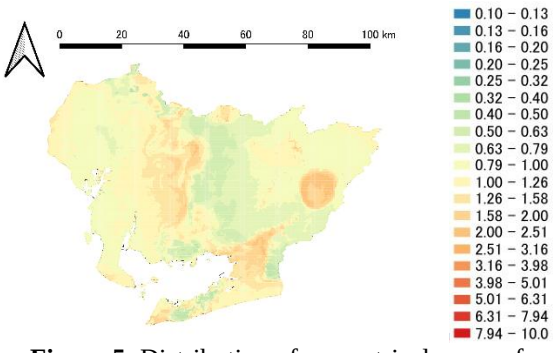

Figure 5: Distribution of geometrical mean of compensation ratios

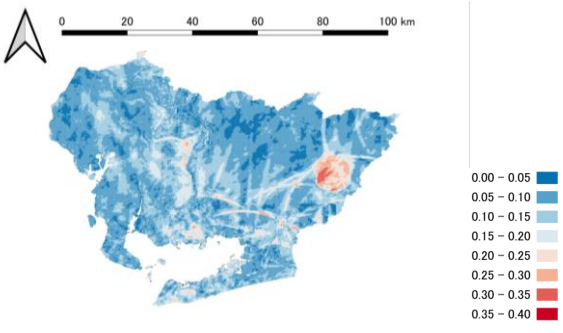

Figure 6: Distribution of coefficient of variation of compensation ratios

Figure 6 shows the spatial distribution of the coefficients of variation for the six compensation ratios calculated across 80,000 mesh points. The results depict that the coefficient of variation is below 0.15 in over 85% of the meshes in Aichi Prefecture, with the maximum value being less than approximately 0.35.

These findings suggest that the random component—the compensation ratio—can be regarded as a site-specific constant independent of the epicenter model or seismic wave direction.

Once a database of compensation ratios is constructed, seismic intensity can be accurately estimated using seismic waves observed or simulated at a limited number of seismometer locations on the engineering bedrock.

5 CONCLUSIONS

In this study, the time-dependent FSI, used as an index of seismic intensity for estimating the seismic risk of houses, was assumed to follow a log-normal random field distribution. The trend component was considered to vary with earthquake source characteristics, whereas the random component, defined as the compensation ratio, was assumed to be independent of those characteristics.

The six sets of compensation ratios derived from the analysis exhibited similar spatial distributions regardless of the seismic source, thereby supporting the validity of this assumption.

These findings suggest that the spatial distribution of FSI on engineering bedrock at arbitrary locations can be accurately estimated using a limited number of seismometers in combination with a pre-established database of compensation ratios.

Constructing a database of the compensation ratios for each natural period is crucial. The accuracy of the proposed method should be validated by comparing the seismic intensities estimated using this database with those observed during actual earthquake events.

ACKNOWLEDGMENT

The authors are deeply appreciative of the funding and encouragement provided by the Japan Construction Information Center. They also gratefully acknowledge the English language editing provided by Editage (www.editage.com), whose careful and professional work contributed to the clarity and accuracy of the manuscript.

REFERENCES

[1] Sugai, M., Mizutani, Y. and Mori, Y. Application of Kriging method to the estimation of seismic hazards for each construction site. *AIJ J. Technol. Des.* (2016) **22**:447-452 (in Japanese).

[2] National Research Institute for Earth Science and Disaster Resilience (https://www.doi.org/10.17598/NIED.0004) (accessed on 30 Dec 2022)

[3] Sugai, M., Mori, Y. and Ogawa, K. Application of Kriging method to practical estimations of earthquake ground motion hazards. *J. Struct. Constr. Eng. AIJ* (2015) 39-46 (in Japanese).

[4] Mizutani, Y., Sugai, M. and Mori, Y. Study on the estimation of earthquake ground motion

at engineering base layer via Kriging method. *Proc., Ann. Meet. Tokai Chapt.* (2017) **55**:189-192. (in Japanese).

[5] Mizutani, Y., Sugai, M. and Mori, Y. Fourier amplitude spectrum at arbitrary points estimated by Kriging method. *13th Int. Conf. Appl. Stat. Prob. Civ. Eng.* Seoul, South Korea, (2019) 468.

[6] Mizutani, Y., Sugai, M. and Mori, Y. Practical estimation method for acceleration Fourier amplitude spectrum at an arbitrary point by using advanced Kriging method. *Proc. 7th Asian-Pacific Symp. Struct. Reliab. Appl.* Tokyo, Japan, MM1-4 (2020).

[7] Sugai, M., Mori, Y. and Mizutani, Y. Practical method for estimating acceleration Fourier amplitude spectrum at an arbitrary point. *Proc. 8th Intl. Symp. Reliab. Eng. Risk Manag*. (2022) 635-639.

[8] Krige, D.G. A Statistical Approach to Some Mine Valuation and Allied Problems on the Witwatersrand. Master's Thesis, University of Witwatersrand, South Africa (1951).

[9] Matheron, G. Principles of geostatistics. *Econ. Geol.* (1963) **58**:1246-1266.

[10] Akaike, H. Selection of prior distribution and its application. *Bayesian, Statistics and Its Applications*, edited by Y. Suzuki and N. Kumamoto, 81-98, Univ. of Tokyo Press, Japan (1989) (in Japanese).

[11] Honda, M. Statistical Approach to Space/Time Prediction and Its Application to Geotechnical Problems. Doctoral thesis, Kyoto University, Japan (2000) (in Japanese).

[12] Ammen, H. and Mori, Y. A study on damage function using Fourier amplitude spectrum intensity as scale of ground motion intensity. *Proc. Ann. Res. Meet. AIJ, Tokai Chapt.* (2025) **62**:77-78 (in Japanese).

[13] Aichi Prefecture Disaster Council Earthquake Subcommittee. Damage Prediction Survey Results including Aichi Prefecture Tokai Earthquake, Tonankai Earthquake (2014) (in Japanese).